137

Shape-Based Classification of Clustered Microcalcifications in Digitized Mammograms

J.K. Kim*, J.M. Park**, K.S. Song**, and H.W. Park

Department of Electrical Engineering, Korea Advanced Institute of Science and Technology
*Software Lab., Corporate R&D Center, Samsung Electronics Co.
**Department of Diagnostic Radiology, Asan Medical Center, University of Ulsan College of Medicine

Abstract : Clustered microcalcifications in X-ray mammograms are an important sign for the diagnosis of breast cancer. A shape-based method, which is based on the morphological features of clustered microcalcifications, is proposed for classifying clustered microcalcifications into benign or malignant categories. To verify the effectiveness of the proposed shape features, clinical mammograms were used to compare the classification performance of the proposed shape features with those of conventional textural features, such as the spatial gray-level dependence method and the wavelet-based method. Image features extracted from these methods were used as inputs to a three-layer backpropagation neural network classifier. The classification performance of features extracted by each method was studied by using receiver operating-characteristics analysis. The proposed shape features were shown to be superior to the conventional textural features with respect to classification accuracy.

Key words : Breast cancer, Clustered microcalcifications, Shape analysis, Receiver operating-characteristics (ROC) analysis, Computer-aided diagnosis

I. INTRODUCTION

Breast cancer is one of the major causes of mortality in middle-aged women, especially in developed country[1]. In 1994, the mortality and the incidence rate of breast cancer were estimated as 3.9 and 9.9 per 100,000 women, respectively, in Korea[2]. The mortality of breast cancer in Korea is lower than that of other developed countries; 33.7 in United States, 10.7 in Japan, 13.8 in Singapore, 35.5 in France, and 44.5 in Germany; however, it continues to slowly increase in Korea[2]. Mammography associated with clinical breast examination is the most effective method for early detection of breast cancer [3]. However, it is very difficult to interpret X-ray mammograms because of the small differences in the image densities of various breast tissues, in particular, for dense

통신저자 : 박현욱, (305-701)대전광역시 유성구 구성동 373-1
한국과학기술원 전기 및 전자공학과
Tel. (042)-869-3466, Fax. (042)869-8066
E-mail. hwpark@athena.kaist.ac.kr

breast[4]. Radiologists interpret mammograms by visual examination of the X-ray films for the presence of abnormalities that can be interpreted as breast cancer. It has been reported that about 10-30% of patients with breast cancer are misdiagnosed by mammography (the cancer is missed or misinterpreted) and only 10-30% of cases that have mammographically suspicious findings prove to be malignant when subjected to biopsy[5].

Calcifications, which are one of the early signatures of breast cancer, are calcium deposits that form on the breast as a result of a benign or a malignant process. Calcifications with diameters of less than 0.7mm are called microcalcifications. It has been reported that 30-50% of breast cancers detected radiographically had the clustered microcalcifications in mammograms, and 60-80% of breast cancers had the clustered microcalcifications upon microscopic examination[6]. Therefore, clustered microcalcifications are an important sign in the detection of breast cancer. The clinical experience of radiologists indicates that clustered microcalcifications are defined as containing three or more microcalcifications within an

area of 1cm×1cm in mammograms[7]. Computer-aided diagnosis (CAD) methods[8-14] for classification of microcalcifications have been proposed to increase the radiologist's sensitivity and specificity and to minimize the number of unnecessary biopsies.

The morphologies of the microcalcifications are the major criteria for distinguishing benign from malignant in terms of diagnosis of radiologist[4]. Benign and malignant microcalcifications in breast tissues can produce similar patterns of calcium deposition. Biopsy is often required for diagnosis since radiographical examination is not certain to differentiate between benign and malignant microcalcifications. Analysis of the size, the shape, the number, and the density of the microcalcifications in a cluster can, however, improve the discrimination accuracy [4]. Malignant microcalcifications are usually variable in size, shape, and density in a cluster. Benign microcalcifications are often rounder, fewer in number, and more uniform in density and size than malignant microcalcifications. The probability of breast cancer also increases with the number of microcalcifications in a cluster. However, no absolute minimum threshold exists.

This paper proposes a shape-based method for classification of clustered microcalcifications into benign or malignant. The method is based on the morphological features of clustered microcalcifications. To verify the effectiveness of the proposed shape features, a study was performed to compare the classification performance of the proposed shape features with conventional textural features, such as the spatial gray-level dependence method (SGLDM)[15] and the wavelet-based method[11]. Image features extracted from these methods were used as inputs to a three-layer backpropagation neural network classifier [16], which classified regions of interest (ROIs) into positive ROIs containing malignant microcalcifications or negative ROIs containing benign microcalcifications. A receiver operating-characteristics (ROC) analysis[17, 18] was employed to evaluate the classification performance of the image features. The area under the ROC curve, A_z, was used as a measure of the classification performance.

The proposed shape-based classification method is described in Section II of this paper. The experimental results and discussions are presented in Section III. Finally, conclusions are given in Section IV.
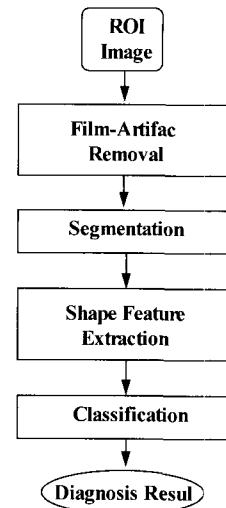

Fig. 1. The block diagram of the proposed shape-based classification

II. SHAPE-BASED CLASSIFICATION METHOD

This section presents the details of the proposed method, which consists of the film-artifact removal, microcalcification segmentation, shape feature extraction, and classification. Figure 1 shows a block diagram of the proposed method for classification of clustered microcalcifications into benign or malignant categories. In Fig. 1, the ROI denotes the breast region containing clustered microcalcifications, which is selected with an area of 128 ×128 pixels from the digitized mammograms.

A. Film-Artifact Removal

There are small emulsion continuity faults on X-ray films, which look like microcalcifications[4]. These artifacts are usually more sharply defined and brighter than the microcalcifications in X-ray mammogram films. A

-1/8	-1/8	-1/8
-1/8	1	-1/8
-1/8	-1/8	-1/8

Fig. 2. 3×3 discrete Laplacian operator

simple film-artifact removal filter is applied to the original digitized image in order to remove the film artifacts. The proposed film-artifact removal filter exploits the fact that the boundaries of the film artifact are abrupt, whereas those of microcalcifications are smooth.

Let us consider a 3×3 window centered on a current pixel (x, y) and compute the gradients at nine points within the window. Each gradient is obtained by a 3×3 discrete Laplacian operator, as shown in Fig. 2. If the maximum gradient, $g_{max}(x, y)$, among the nine gradients is larger than a threshold value, T_g, the current pixel at the center of the 3×3 window is regarded as the film artifact and is replaced by the median value of the pixels within a 5×5 window W. The output of the film-artifact removal filtering, $S(x, y)$, is defined as

$$S(x,y) = \begin{cases} \text{median}\{I(x-k, y-l), (k,l) \in W\}, & \text{if } g_{max}(x,y) > T_g \\ I(x,y), & \text{otherwise} \end{cases} \quad (1)$$

where $I(x, y)$ is the original image and W is the 5×5 window. In eq. (1), the threshold value, T_g, is empirically selected from many digitized mammograms so that the film artifacts can be removed and the microcalcifications can be preserved.

B. Segmentation of Microcalcifications

In general, the shape-based classification can be performed by using the binary information representing microcalcifications. Shape feature extraction is then performed from such segmented binary images. Therefore, the performance of shape-based classification depends on
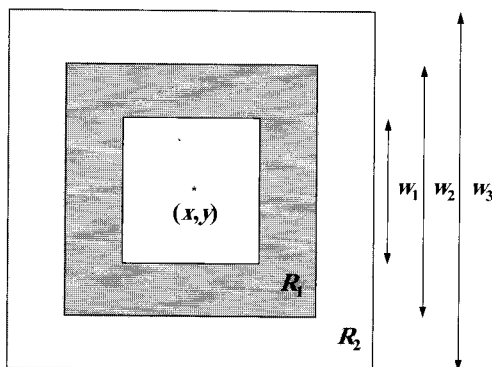

Fig. 3. Configuration of the surrounding regions centered at the current pixel (x, y). R_1 and R_2 are the inner surrounding region and the outer surrounding region, respectively. w_1, w_2, and w_3 denote the size of each square window

the segmentation of the microcalcifications. A segmentation method is proposed to extract the original shapes of the microcalcifications in the ROIs containing clustered microcalcifications.

Let us consider three rectangular windows centered on a current pixel (x, y), as shown in Fig. 3. In this figure, R_1 and R_2 are the inner surrounding region and the outer surrounding region, respectively, and w_1, w_2, and w_3 denote the size of each square region. In this study, w_1, w_2, and w_3 have the values of 3, 5, and 7, respectively. These window sizes are determined in consideration of the lesion size to be detected and the pixel resolution of digitized X-ray mammograms. The inner count, $C_{R_1}(x,y)$, and the outer count, $C_{R_2}(x,y)$, on the current pixel (x, y) are defined as follows,

$$c_{R_1}(x,y) = \#\{(k,l)|(k,l) \in R_1 \text{ and } |S(x,y) - S(k,l)| > q\} \quad (2)$$

$$c_{R_2}(x,y) = \#\{(k,l)|(k,l) \in R_2 \text{ and } |S(x,y) - S(k,l)| > q\} \quad (3)$$

where # denotes the number of elements in the set, $S(x, y)$ is the image intensity on the current pixel (x, y), and q is a given threshold value. The q value is determined empirically so that the original shapes of the microcalcifications can be preserved. Segmentation of individual microcalcifications is performed by thresholding the inner count and the outer count of eqs. (2) and (3) to decide whether a pixel belongs to a microcalcification. The binary image $B(x, y)$ is computed as follows,

$$B(x,y) = \begin{cases} 1, & \text{if } c_{R_1}(x,y) \geq T_1 \text{ or } c_{R_2}(x,y) \geq T_2 \\ 0, & \text{otherwise} \end{cases} \quad (4)$$

where T_1 and T_2 are the threshold values of the inner count and the outer count, respectively. In our study, T_1 and T_2 have values of 8 and 12, respectively, to differentiate the pixels in the microcalcifications from the pixels in the normal tissues. In the binary image obtained from eq. (4), "1" means the pixel is in a microcalcification region. However, small objects less than four pixels are excluded from the microcalcifications because very small objects are usually noise caused by inhomogeneous tissue background.

C. Shape Feature Extraction

The shape features employed in this study are based on the morphological features of clustered microcalci-

fications and are derived from the binary image B(x, y). Four shape features are used in order to describe the visibility and the shape of the individual microcalcifications; these are the size, the mean density, the ratio of the semimajor to the semiminor axes of the best-fit ellipse, and the eccentricity.

The size (or area) is defined as the number of pixels contained within the microcalcification region. The mean density of the individual microcalcification is defined as the average of the original pixel values S(x, y) in the microcalcification region. The best-fit ellipse and the eccentricity are useful shape features[19], which are based on the moment of the object. For an object represented by a region R containing N pixels, the center of mass is given by

$$\bar{x} = \frac{1}{N}\sum_{(x,y)\in R} x, \quad \bar{y} = \frac{1}{N}\sum_{(x,y)\in R} y \tag{5}$$

The (p+q)-order central moment becomes

$$\mu_{pq} = \sum\sum_{(x,y)\in R}(x-\bar{x})^p(y-\bar{y})^q. \tag{6}$$

The object orientation θ is the angle between the major axis of the object and the x axis, which is defined as follows,

$$\theta = \frac{1}{2}\tan^{-1}\left[\frac{2\mu_{11}}{\mu_{20}-\mu_{02}}\right]. \tag{7}$$

The ratio, a/b, of the semimajor to the semiminor axes of the best-fit ellipse is calculated as follows: The best-fit ellipse is the ellipse whose second moment as equal to that of the object. Let a and b denote the lengths of the semimajor and the semiminor axes, respectively, of the best-fit ellipse. For the best-fit ellipse, a and b are given as follows,

$$a = \left(\frac{4}{\pi}\right)^{\frac{1}{4}}\left[\frac{(I_{max})^3}{I_{min}}\right]^{\frac{1}{8}}, \quad b = \left(\frac{4}{\pi}\right)^{\frac{1}{4}}\left[\frac{(I_{min})^3}{I_{max}}\right]^{\frac{1}{8}} \tag{8}$$

where I_{max} and I_{min} can be calculated as

$$I_{max} = \sum\sum_{(x,y)\in R}\left[(x-\bar{x})\sin\theta+(y-\bar{y})\cos\theta\right]^2, \tag{9}$$

Table 1. Shape features for classification of clustered microcalcifications into benign or malignant.

| Morphologies of individual microcalcifications |
| --- |
| Size |
| Mean density |
| Ratio of the semimajor to the semiminor axes of the best-fit ellipse |
| Eccentricity |
| Shape features of clustered microcalcifications |
| Mean of above measurements in an ROI |
| Standard deviation of above measurements in an ROI |
| Maximum of above measurements in an ROI |
| (Maximum - Mean) of above measurements in an ROI |
| (Mean - Minimum) of above measurements in an ROI |
| Number of microcalcifications in an ROI |

$$I_{min} = \sum\sum_{(x,y)\in R}\left[(x-\bar{x})\cos\theta-(y-\bar{y})\sin\theta\right]^2. \tag{10}$$

Finally the object eccentricity is defined as follows,

$$\varepsilon = \frac{(\mu_{20}-\mu_{02})^2+4\mu_{11}}{area}. \tag{11}$$

The above features are taken for each microcalcification. In order to describe the variations of the morphologies of the microcalcifications in an ROI, the mean, the standard deviation, the maximum, the difference between the maximum and the mean, and the difference between the mean and the minimum are calculated from these features. A total of twenty-one shape features, including the number of microcalcifications in an ROI, are extracted, as listed in Table 1.

D. Classification
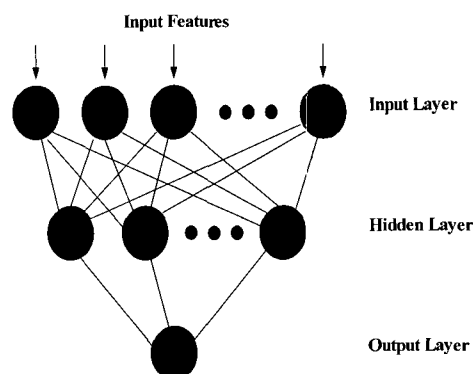
Fig. 4. Structure of the three-layer backpropagation neural network

In order to classify ROIs into positive ROIs containing malignant microcalcifications or negative ROIs containing benign microcalcifications, a three-layer backpropagation neural network [16] is employed as a classifier, as shown in Fig. 4. A nonlinear sigmoid function with "0" and "1" saturation values is used as the activation function for each neuron.

In the training process, the weights between the neurons are adjusted iteratively so that the difference between the output values and the target values is minimized. The weight values are updated by iteration as follows,

$$w_{ji}(l+1) = w_{ji}(l) + \eta \delta_j o_i + \mu \left[w_{ji}(l) - w_{ji}(l-1) \right] \qquad (12)$$

where w_{ji} (l) is the weight from the ith to the jth neurons, o_j is the jth element of the actual output pattern produced by an input pattern, η is the learning rate, l is the number of epochs, δ_j is the error signal, and μ is a momentum parameter. To evaluate the network performance during the training process, a global error measure [20] is given as

$$\varepsilon_{RMS} = \sqrt{\frac{\sum_{g=1}^{G} \left[o_g - t_g \right]^2}{G}} \qquad (13)$$

where o_g and t_g are the output and the target values for the gth input pattern, respectively, and G is the number of training patterns. In this study, the training process is stopped when the root mean square (RMS) error, ε_{RMS}, becomes smaller than a given constant ε_0.

III. EXPERIMENTAL RESULTS AND DISCUSSION

A. ROI Selection

From the patient files in the Department of Radiology at Asan Medical Center in Seoul, Korea, one hundred fourteen X-ray mammograms with clustered microcalcifications were selected. The mammograms were digitized by a Lumisys laser film scanner with a pixel size of 100 μm×100 μm and 12 bits per pixel. One hundred fourteen ROIs were selected from the database of digitized mammograms. An ROI was selected with an area of 128×128 pixels (i.e., 1.28cm×1.28cm) from the digitized mam-
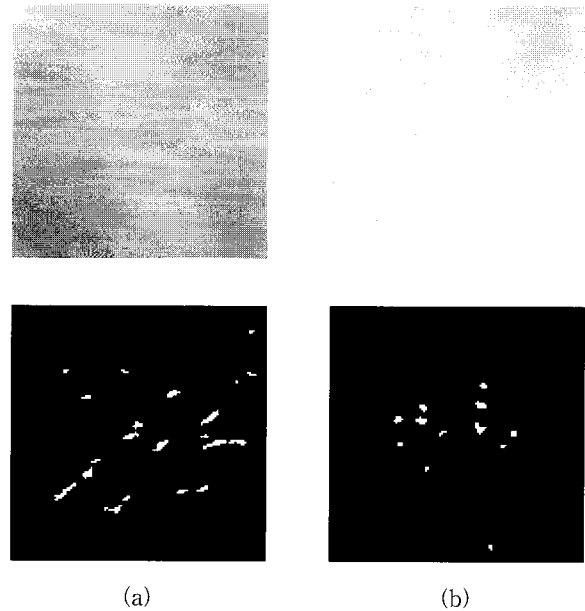

(a)   (b)

Fig. 5. Examples of segmented microcalcifications in ROI images with 128×128 pixels: (a) positive ROI and (b) negative ROI. The computation was performed when the threshold q was 60, and w_1, w_2, and w_3 were 3, 5, and 7, respectively
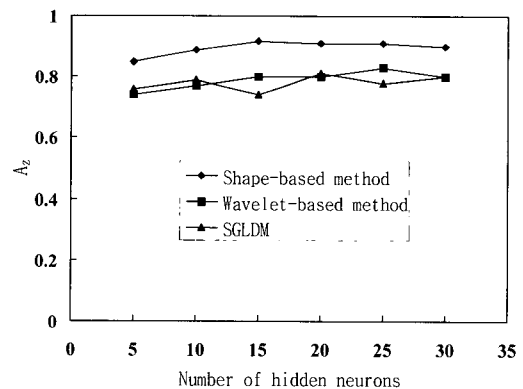

Fig. 6. Area under the ROC curve, A_z, to define the optimum number of hidden neurons for each classification method. A_z values were computed for various numbers of hidden neurons (i.e., 5, 10, 15, 20, 25, and 30 neurons) in order to find the optimum number of hidden neurons

mograms, and all of the ROIs included clustered microcalcifications.

Among the selected 114 ROIs, 62 ROIs were positive, i.e., contained malignant microcalcifications, and 52 ROIs were negative, i.e., contained benign microcalcifications. Benign or malignant of clustered microcalcifications were verified by an expert mammographer.

B. Comparative Study

To study the efficacies of classification, the proposed method was compared with conventional textural methods, such as the SGLDM and the wavelet-based method. The SGLDM [15], which has been widely used in pattern recognition fields, is based on an estimate of the second-order joint conditional probability density functions, $p(i, j|d, \theta)$, for $\theta = 0°$, $45°$, $90°$, and $135°$. The function $p(i, j|d, \theta)$ is the probability that two pixels, which are located with an intersample distance d and a direction θ, have a gray-level i and a gray-level j. Each of the estimated joint probability density functions can be written in matrix form; i.e., the spatial gray-level dependence matrix, $\Phi(d, \theta)$, which is given as follows,

$$\Phi(d, \theta) = [p(ij|d, \theta)], \quad 0 \le i,j \le N_g \qquad (14)$$

where N_g is the maximum gray-level. Thirteen textural features are measured from the matrix $\Phi(d, \theta)$; *energy, entropy, correlation, local homogeneity, inertia, sum average, sum variance, sum entropy, difference average, difference variance, difference entropy, information measure of correlation 1, and information measure of correlation 2* [15]. In this study, four spatial gray-level dependence matrices for four different directions ($\theta = 0°$, $45°$, $90°$, and $135°$) are obtained at $d = 1$. A total of 52 textural features are calculated for an ROI. These fifty-two textural features are used as input to the classifier.

Kocur et al [11] explored the usefulness of wavelet analysis for the classification of benign and malignant microcalcifications by using Daubechies-4, Daubechies-20, and biorthogonal wavelets. An ROI is decomposed into four matrices, such as the approximation signal and the horizontal, vertical, and diagonal detail coefficients. Multilevel wavelet analysis decomposes the approximation signal further and repeats the decomposition until a single pixel depiction results. At each level, the decomposed coefficients are squared and summed, and the square root is taken to generate a single feature for each of the approximation and details of that level. The wavelet-based method is investigated by computing the wavelet transform in the ROI. Therefore, these sets of four numbers for each level, a total of 28 wavelet features, are calculated for an ROI and are used as input to the classifier. In this study, the Daubechies-4 wavelet is employed.

The proposed shape-based method is based on the

morphological features of clustered microcalcifications. In this experiment, the threshold values T_g and q had value of 110 and 60, respectively. Figure 5 shows examples of segmented microcalcifications for a positive ROI and a negative ROI. Shape features are derived from the segmented microcalcifications in an ROI. To describe the variations of the morphologies of the microcalcifications in an ROI, a total of 21 shape features are calculated for an ROI, as described in Section II, and are used as input to the classifier.

A three-layer backpropagation neural network was employed as a classifier, as described in Section II. The neural networks were tested by using a round-robin method[21]. When there are P sample patterns, the round-robin method trains the classifier with $P-1$ samples, then uses the one remaining sample as a test sample. Classification is repeated in this manner until all P samples have been used once as a test sample. In this study, P was 114 (114 sample ROIs). Since the round-robin method is performed with the sample which is not used for training the neural network, these trials provide a good approximation of the general performance of the neural network. All the textural features were normalized by the sample mean and standard deviation of the data set. Each training of the neural network was stopped whenever ε_{RMS} was less than 0.1 in this experiment, i.e., ε_0 was 0.1. The learning rate and the momentum had values of 0.08 and 0.7, respectively. The results of the backpropagation neural network were analyzed by using an ROC analysis. The ROC analysis was employed to evaluate the performance of the image features in classifying the ROIs into positive and negative ROIs. ROC curves were obtained by using LABROC1 program developed by Metz et al [22] to fit the continuous outputs of the neural networks. The area under the ROC curve, A_z, was used as a measure of the classification performance.

In order to obtain the best classification performance for the neural network, the optimum number of hidden neurons in the neural network was analyzed for each method of feature extraction. Figure 6 shows the results of the classification performances with respect to the number of neurons in the hidden layer of the backpropagation neural network. The neural network for the proposed shape-based method has 15 hidden neurons, the wavelet-based method has 25 hidden neurons, and the neural network for the SGLDM has 20 hidden neurons for optimum classification performance. Figure 7 shows a
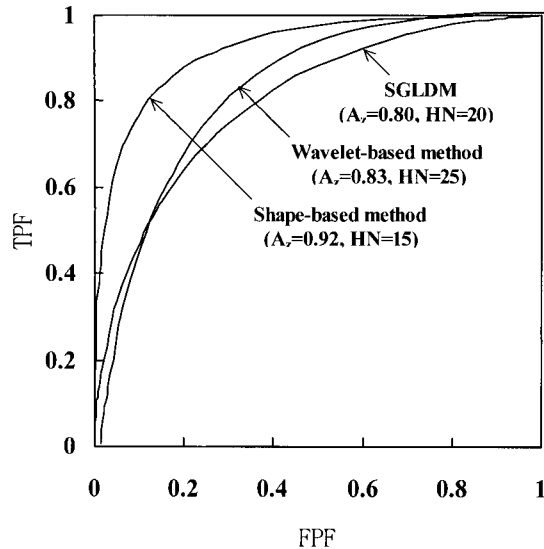
Fig. 7. Comparison by the round-robin method of ROC curves for the optimal performance of each method. TPF and FPF are the true-positive fraction and the false-positive fraction, respectively. A_z values of the SGLDM (at HN = 20), the wavelet-based method (at HN = 25), and the proposed shape-based method (at HN = 15) are 0.80, 0.83, and 0.92, respectively. HN denotes the number of hidden neurons

comparison of the ROC curves for each feature extraction method with the optimum number of hidden neurons. In Fig. 7, TPF and FPF are the true-positive fraction and the false-positive fraction, respectively. A_z values of the SGLDM, the wavelet-based method, and the proposed shape-based method are 0.80, 0.83, and 0.92, respectively. From the viewpoint of classification accuracy, it is apparent that the proposed shape features have the best performance for classification of clustered microcalcifications into benign or malignant categories.

IV. CONCLUSIONS

This paper proposed a shape-based method for classification of clustered microcalcifications into benign or malignant. Twenty-one shape features were defined, which were based on the morphological features of clustered microcalcifications. A three-layer backpropagation neural network was employed as a classifier. To verify the usefulness of the proposed shape features for classification of clustered microcalcifications, we compared the classification performance of the proposed shape features with those of two conventional methods in terms of ROC analysis. The proposed shape features were superior to the conventional methods with respect to classification

performance.

In spite of the limited number of cases, the experimental results for the proposed method are promising. However, a comprehensive database that covers a lot of positive ROIs and negative ROIs will be needed for the training of the neural network in order to apply this method to clinical situations involving the classification of clustered microcalcifications in mammograms. In addition, we will compare whether the overall performance may be improved by combining the proposed shape features with the textural features or not, and the thresholds in the proposed segmentation algorithm will be tuned in order to further improve the classification performance.

REFERENCES

1. R.G. Bird, R.G. Wallace, and B.C. Yankaskas, "Analysis of cancers missed at screening mammography", Radiology, Vol. 184, pp. 613-617, 1992

2. Y.O. Ahn, B.J. Park, and K.Y. Yoo, "Incidence estimation of female breast cancer among Koreans", Journal of Korean Med. Sci., Vol. 9, pp. 328-334, 1994

3. P.C. Johns and M.J. Yaffe, "X-ray characterization of normal and neoplastic breast tissues", Phys. in Med. and Biol., Vol. 32, pp. 675-695, 1987

4. D.B. Kopans, Breast Imaging, Lippincoff Company, Philadelphia, 1989.

5. F.M. Hall, J.M. Storella, D.Z. Silverstone et al., "Nonpalpable breast lesions: Recommendations for biopsy based on suspicion of carcinoma at mammography", Radiology, Vol. 167, pp. 353-358, 1988

6. H.P. Chan, K. Doi, S. Galhotra et al., "Image feature analysis and computer-aided diagnosis in digital radiography. 1. Automated detection of microcalcifications in mammography", Med. Phys., Vol. 14, pp. 538-548, 1987

7. M. Lanyi, Diagnosis and Differential Diagnosis of Breast Calcifications, Springer-Verlag, Berlin, 1988

8. J.K. Kim, J.M. Park, K.S. Song, and H.W. Park, "Detection of clustered microcalcifications on mammograms using surrounding region dependence method and artificial neural network", Journal of VLSI Signal Processing, Vol. 18, pp. 251-262, 1998

9. L. Shen, R.M. Rangayyan, and J.E. L. Desautels, "Application of shape analysis to mammographic calcifications", IEEE Trans. Med. Imag, Vol. 13, pp. 263-274, 1994

10. A.P. Dhawan, Y. Chitre, C.K. Bonasso et al., *"Analysis of mammographic microcalcifications using gray-level image structure features"*, IEEE Trans. Med. Imag. Vol. 15, pp. 246-259, 1996

11. C.M. Kocur, S.K. Rogers, L.R. Myers et al., *"Using neural networks to select wavelet features for breast cancer diagnosis"*, IEEE Eng. in Med. and Biol., pp. 95-102, May/June 1996

12. O. Tsujii, A. Hasegawa, C.Y. Wu et al., *"Classification of microcalcifications in digital mammograms for the diagnosis of breast cancer"*, Proc. SPIE Medical Imaging, Vol. 2710, pp. 794-804, 1996

13. H.P. Chan, B. Sahiner, N. Petrick et al., *"Effects of pixel size on classification of microcalcifications on digitized mammograms"*, Proc. SPIE Medical Imaging, Vol. 2710, pp. 30-41, 1996

14. M.A. Gavrielides, M. Kallergi, and L.P. Clarke, *"Automatic shape analysis and classification of mammographic calcifications"*, Proc. SPIE Medical Imaging, Vol. 3034, pp. 869-876, 1997

15. R.M. Haralick, K. Shanmugan, and I. Dinstein, *"Textural features for image classification"*, IEEE Trans. Syst. Man and Cybern, Vol. SMC-3, pp. 610-621, 1973

16. L. Fausett, Fundamentals of Neural Networks, Prentice-Hall, Englewood Cliffs, NJ, 1994

17. C.E. Metz, *"ROC methodology in radiologic imaging"*, Investigative Radiology, Vol. 21, pp. 720-733, 1986

18. C.E. Metz, *"Some practical issues of experimental design and data analysis in radiological ROC studies"*, Investigative Radiology, Vol. 24, pp. 234-245, 1989

19. A.K. Jain, Fundamentals of Digital Image Processing, Prentice-Hall, Englewood Cliffs, NJ, 1989

20. K.R. Castleman, Digital Image Processing, Prentice-Hall, Englewood Cliffs, NJ, 1996

21. M. Nadler and E.P. Smith, Pattern Recognition Engineering, Wiley, New York, 1993

22. C.E. Metz, J.H. Shen, and B.A. Herman, *"New methods for estimating a binormal ROC curve from continuously-distributed test results"*, presented at the 1990 Annual Meeting of the American Statistical Association, Anaheim, CA, Aug. 1990